Received: 14 March 2023 | Accepted: 5 July 2023 | Published online: 20 July 2023

DOI: 10.1111/opo.13203

OPO THE COLLEGE OF OPTOMETRISTS

ORIGINAL ARTICLE

Using a video-based eye tracker to analyse the binocular near-reflex dynamics response

Julián Espinosa[1,2] | **Kauzar Archid**[1] | **Jorge Pérez**[1,2] | **Esther Perales**[1,2]

[1]Departamento de Óptica, Farmacología y Anatomía, Universidad de Alicante, Alicante, Spain

[2]Instituto Universitario de Física, Aplicada a las Ciencias y las Tecnologías, Universidad de Alicante, Alicante, Spain

Correspondence
Julián Espinosa, Departamento de Óptica, Farmacología y Anatomía, Instituto Universitario de Física, Aplicada a las Ciencias y las Tecnologías, Universidad de Alicante, Alicante, Spain.
Email: julian.espinosa@ua.es

Funding information
Universidad de Alicante, participating CRUE-CSIC institution

Abstract

Purpose: This study presents a novel video-based eye-tracking system for analysing the dynamics of the binocular near-reflex response. The system enables the simultaneous measurement of convergence, divergence and pupillary size during accommodation and disaccommodation to aid the comprehensive understanding of the three-component near-reflex.

Methods: A high-speed (90 Hz) video-based eye tracker was used to capture changes in eye gaze and pupil radius in 15 participants in response to altering stimulus conditions. An offline analysis involved separating the gaze vector components and pupil radius, which were fitted to a hyperbolic tangent function to characterise the dynamics of the near-reflex process.

Results: Significant differences in the temporal parameters of the pupil radius were observed between the near-to-far and far-to-near vision changes, with faster miosis compared with mydriasis. Additionally, differences in response times were found between gaze angle components, with longer convergence times compared to changes in the vertical direction (saccades). The steady-state values of the gaze components and pupil radius were in line with theoretical expectations and previous reports.

Conclusions: The proposed system provides a non-invasive, portable and cost-effective method for evaluating near-reflex dynamics under natural viewing conditions using a video-based eye tracker. The sampling rate ensures the accurate assessment of vergence eye movements and pupillary dynamics. By simultaneously measuring eye convergence, divergence and pupil size, the system offers a more comprehensive assessment of the near-reflex response. This makes it a valuable tool for clinical diagnosis, research studies and investigating the effects of near work on the visual system.

KEYWORDS
accommodation, convergence, near-reflex response, pupillary accommodation, video-based eye tracker

INTRODUCTION

A change in fixation from a distant to a near object elicits the near reflex, which is a three-component reflex that comprises pupillary constriction (miosis), lens accommodation and convergence.[1–4] Pupillary constriction (miosis) increases the eye's depth of focus while accommodation produced increased lens curvature, with an increase in refractive power. The eyes converge to position the retinal image on the fovea of each eye.

The convergence accommodation-to-convergence (CA/C) ratio represents the relationship between disparity vergence and the resulting accommodative response.[5] Additionally, under binocular viewing conditions, the CA/C ratio interacts with the accommodative convergence-to-accommodation (AC/A) ratio.[6–8] Both ratios contribute to

the adaptive and cross-linking interactions between these two motor systems. However, it is important to note that relying solely on either ratio will provide an incomplete analysis of these intricate interactions. The typical AC/A ratio has been historically based on the assumption that at a 1-m viewing distance, someone with an interpupillary distance (IPD) of 6 cm will exert 6 prism dioptres (Δ) of convergence, two-thirds of which will be driven by accommodative convergence to yield a normal AC/A of 4Δ:1D.[9] The normal range is between 3 and 5Δ/D to consider differing IPD measurements. Changing from near to distant viewing will produce ocular disaccommodation, divergence and pupil dilation (mydriasis).

The efferent limb of the accommodation reflex has two components, the Edinger–Westphal nucleus, which sends axons in the oculomotor nerve to the ciliary ganglion, which, in turn, sends axons in the short ciliary nerve to control the iris sphincter and the crystalline lens. Furthermore, oculomotor neurons send axons in the oculomotor nerve to control the convergence of each eye. Thus, the ciliary muscle, sphincter pupillae and medial rectus muscles are involved in the near-triad response.

Vergence oculomotor plant control has been reported to involve a dual-mode strategy.[10–13] This consists of an open-loop, fusion-initiating component that drives the initial vergence movements by facilitating the alignment of the visual axes. This fusion-initiating component is driven by sensory inputs such as retinal disparity and interocular spatial relations, and serves to rapidly bring about the desired vergence response.[14] Following the fusion-initiating phase, a fusion-sustaining component comes into play, driven by visual and internal feedback mechanisms. This component aims to maintain stable binocular vision. Visual feedback includes ongoing retinal disparity information and other depth cues, which continuously contribute to the fine-tuning of vergence movements.[15] However, internal feedback, involving proprioceptive signals and neural adaptation processes optimise the vergence system's performance over time.[16]

By employing this dual-mode strategy, the vergence plant effectively coordinates the complex interaction between the visual system and the extraocular muscles by ensuring accurate binocular alignment and depth perception. Understanding the interplay between the accommodation neurophysiology and vergence plant dynamics is crucial for comprehending the mechanisms that underlie binocular vision and the adaptive processes that contribute to maintaining a clear and single visual image.

Epidemiological studies have shown a significant correlation between the accommodative effort required during near work and the onset and progression of myopia.[17–19] This is an obvious reason for analysing the dynamics of the accommodative process. Furthermore, an understanding of accommodation and pupil dynamics can help to improve the diagnosis of a variety of visual system disorders, as well as the autonomic and central nervous system.[20]

Key points

- A portable high-speed video-based eye-tracking platform enables the analysis of pupil radius and angle of gaze during accommodation, revealing dynamic parameters under natural viewing conditions.
- Notable findings include significant differences in the temporal parameters of the pupil radius during changes between far and near viewing.
- Comparison of temporal parameters reveals unique dynamics between pupillary radii and gaze vector components, highlighting the differential roles of convergence and saccades in visual processes.

Many previous studies were concerned about ocular accommodation, which can be measured by subjective or objective techniques based on increasing the accommodative demand of a fixation target until it begins to blur,[21] dynamic retinoscopy,[22] autorefractors,[23] wavefront sensors aberrometers[24] or an assessment of retinal image quality calculated using the wavefront[25] or the double-pass technique.[26,27] Studies examining the monocular or binocular dynamics of accommodation have frequently used sympathomimetic drugs to achieve pupil dilation. Typically evaluated parameters include reaction time (latency), that is, the period following initiation of a stimulus before a change in the accommodation response is observed, and response time, that is, the duration from the end of the reaction time to when the steady-state response is achieved. Other parameters such as velocity and acceleration have also been reported.[28–30] Time parameters can be determined from the points at which the response starts and ends,[31–36] using threshold methods,[30,37,38] fitting an exponential function[28,29] that also requires manual determination of the onset of accommodation or a threshold definition and fitting to a Boltzmann sigmoidal function.[39,40]

Analysis of ocular convergence and pupil dynamics are less widespread despite their association. Previous studies have simultaneously examined accommodation and vergence,[30] pupil reactions and accommodation[41] and the complete triad under natural viewing conditions.[38] Video-based devices (e.g., optometers and eye trackers) are commonly used for this purpose.[30,38,41,42] The associations between pupillary miosis and ciliary innervation lead to the hypothesis that observations of these responses might reveal useful information on the characteristics of the three-component near reflex,[43] including accommodation. In this work, we developed a video-based eye tracker to simultaneously measure convergence and pupil size during accommodation and disaccommodation at high speed and under natural viewing conditions. We developed a calibration process and computed a set of

parameters that describe the dynamics of these processes following changes in fixation. The method's potential and accuracy were evaluated by comparing the results, not only to theoretical angular deviation values but also to previously published data.

METHODS

Subjects

Fifteen subjects (eight females and seven males) participated in this study with a mean age (standard deviation, SD) of 24 (4) years. This study followed the Declaration of Helsinki principles, adhered to the ethical principles of the University of Alicante and participants gave written informed consent regarding the aims, procedures and possible risks before performing the experiment. Every subject had best-corrected visual acuity of logMAR 0.0 (6/6) or better in each eye, as determined by non-cycloplegic subjective refraction. None had ocular disease or artificial intraocular lenses, and none had undergone ophthalmic surgery. Any subject with fixation difficulties or binocular vision dysfunction was excluded from the experiment.

The experimental setup principally consisted of a Pupil Core's eye-tracking platform[44] (Pupil Labs GmbH, pupil-labs.com/products/core/) working at 90 Hz, two Apple MacBook Air 1.7 GHz Intel Core i5, 11.6″ (1366 × 768 Pixels; apple.com) and a 17″ LED screen (1280 × 1024 Pixels; Acer K222HQL, store.acer.com/index.html). Subjects were positioned in a chinrest and faced two displays placed at distances of 33 cm (near) and 4 m (far). By considering the eye as a spherical globe (radius 1.2 cm), then the distance from the near display to a plane containing the centres of the eyes and parallel to the displays was $d_{N-E} = 34.2$ cm, while the distance from the far to the near display was $d_{F-N} = 367$ cm. A diagram of the experimental setup is shown in Figure 1.

A sequence to induce and assess changes in gaze angle and pupil radius while the eyes accommodated and disaccommodated was designed using Matlab R2022a (mathworks.com). The target was a white-on-black wind rose that subtended an angle of 1.3°. The target was alternatively presented on the far and near displays for 3 cycles, remaining for 4 s in each position. The respective accommodative stimulus were 0.25 D and 2.92 D (i.e., a change of 2.67 D). However, under binocular viewing conditions, the accommodative response was approximately 0.9 times the accommodative stimulus.[45,46] Thus, the accommodative response could be around 2.4 D, that is, the result of a 2.67 D change in accommodation multiplied by 0.9 times this accommodative stimulus.

Note that the target positions were always below the eyes' centre line and the near-distance display did not obstruct the far-distance display. The angular subtense in relation to the horizontal plane Π (containing the eyes' centres) and perpendicular to plane Π at the middle distance between the eyes' centres were $\omega_F = 0.93°$ and $\omega_N = 7°$ for the far and near distances, respectively. The vertical angular subtense of the target in the near and far positions in relation to plane Π, but on the plane perpendicular to plane Π in the pupillary centre position, that is, ε_N and ε_F, respectively, can be obtained with Equations (1) and (2), where *NPD* is the nasopupillary distance, h_{F-E} and h_{N-E} are the difference in height between the line joining the centres of the eyes and the test in the far display, and in the upper position of the near display, respectively, d_{FN} is the distance from the far to the near display and d_{NE} is the distance from the near display to a plane containing the centres of the eyes and parallel to the displays (see Figure 1).

$$\varepsilon_N = \tan^{-1}\left(\frac{h_{N-E}}{l_N}\right); \text{with } l_N = \sqrt{{d_{NE}}^2 + NPD^2}. \quad (1)$$

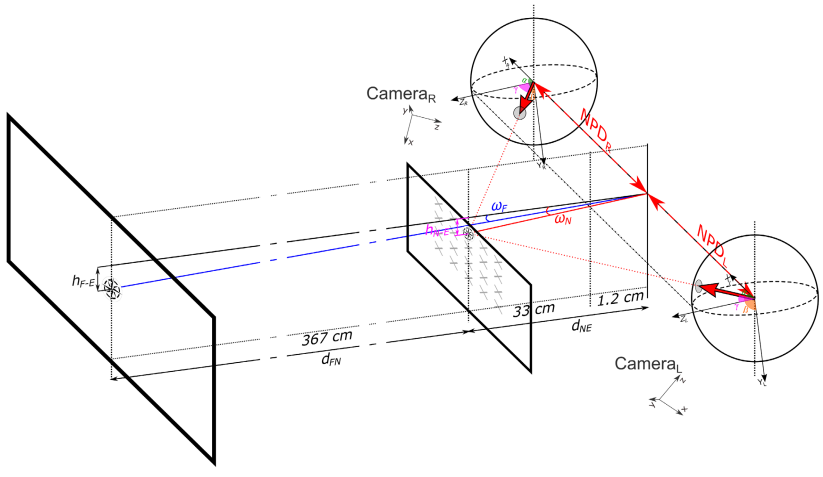

FIGURE 1 Schematic diagram of the experimental setup. h_{F-E} and h_{N-E}, respectively, are the difference in height between the line joining the centres of the eyes and the test in the far display, and in the upper position of the near display, d_{FN} is the distance from the far to the near display, d_{NE} is the distance from the near display to a plane containing the centres of the eyes and parallel to the displays, the nasopupillary distances of the right and left eyes are denoted NPD_R and NPD_L, respectively, while the respective angular subtense in relation to the horizontal plane containing the eyes' centres for the far and near distances are ω_F and ω_N.

Similarly,

$$\varepsilon_F = \tan^{-1}\left(\frac{h_{F-E}}{l_F}\right); \text{with } l_F = \sqrt{\left(d_{FN}+d_{NE}\right)^2 + NPD^2}. \quad (2)$$

The Pupil Core was plugged into one MacBook computer. The other computer was used as a near-distance display and to drive the 17″ LED screen placed at a far distance. The Pupil Core software provides comma-separated values data files that include the direction that the pupil points to in three-dimensional space; that is, the components of the normal vector joining the eye's centre to the pupil's centre and the pupil's radius. Our device lacked the 'world camera'; a frontal camera that records the viewing scene, and is needed to calibrate the device using commercial software. Therefore, we did not have direct gaze data. The reference system used by the device was centred on the charged-coupled device (CCD) of the cameras, which is a disadvantage because the camera positions and orientations were unknown. This drawback was overcome by a calibration procedure, which consisted of defining new coordinates systems' centre for each eye's spherical model, (X_R, Y_R, Z_R) and (X_L, Y_L, Z_L), and obtaining the coordinate system transformation matrices from those centred on the cameras to the new positions. The newly defined reference systems' Z axes (Z_R and Z_L) pointed to the upper target row and were perpendicular to the nasal-temporal line. The X-axis pointed to the nasal direction for the left eye (X_L) and the temporal direction for the right eye (X_R). The Y-axes (Y_R and Y_L) were perpendicular to the Z- and X-axes. In this way, the X-axis gaze angle was related to the eye's convergence angle.

Calibration procedure

A sequence with the target placed at different pre-established positions was proposed as the calibration sequence. During this sequence, the target was moved arbitrarily across the near-distance display both horizontally and vertically in 20 positions (4 rows, 5 columns), separated by an angle of $\omega = 3°$. The target remained at each position for 3 s (the grey crosses in Figure 1).

The positions of the target in the calibration matrix on the near display were established by considering angle ω_N and subtending a constant angle $\omega = 3°$ between neighbouring targets. By denoting columns (left to right) and rows (up to down) with indices, $p = -2, -1, 0, 1, 2$ and $q = 0, 1, 2, 3$, respectively, the target was presented in different positions $(x_{p,q}, y_q)$, defined by the following Equations (3a), (3b) and (3c).

$$z_q = z_0\left(1 + \frac{\sin(q \bullet \omega)\sin(\omega_N)}{\cos(q \bullet \omega + \omega_N)}\right); \text{with } z_0 = \sqrt{{h_{N-E}}^2 + {d_{NE}}^2}; \quad (3a)$$

$$y_q = \frac{z_q - z_0}{\tan(\omega_N)}; \quad (3b)$$

$$x_{p,q} = z_q \tan(p \bullet \omega); \quad (3c)$$

The theoretical directions that the vector gaze pointed to in three-dimensional space for any target position and for each eye-centred reference system can be defined from equations (3a), (3b), (3c) and the nasopupillary distances (NPD). The respective distances of the right and left eyes (NPD_R and NPD_L) were measured with an Essilor digital pupillometer (essilor-instruments.com/product-digital-pupillometer).

The participating subjects were asked to follow the target. The gaze vector components in three-dimensional space data were registered from both eyes. Then, by comparing the theoretical and the registered gaze vectors, two coordinate system transformation matrices (one per eye) were obtained by the least squares fitting technique according to Horn's method based on quaternions.[47]

Data analysis

Sequences were processed offline. The calibration accommodation–disaccomodation sequence generated during each measurement session was recorded in one computer, while the Pupil Core recording was stored by the other computer. The time synchrony of both measurements was confirmed by matching the UNIX Epoch time from each computer. Thus, the exact times when targets were displayed in each position were registered. They slightly differed from the theoretical values due to delays in the plotting of targets.

The registered gaze vector direction throughout the sequence was transformed into the new reference system using the transformation matrices obtained during the calibration process. These gaze vector components (v_x, v_y, v_z) were used to quantify the direction angles (Equation 4) of the gaze line:

$$\alpha = \cos^{-1}\left(\frac{v_x}{\|v\|}\right); \beta = \cos^{-1}\left(\frac{v_y}{\|v\|}\right); \gamma = \cos^{-1}\left(\frac{v_z}{\|v\|}\right); \quad (4)$$

where $\|v\| = \sqrt{v_x^2 + v_y^2 + v_z^2}$. Convergence is related to angle α, but it is important to consider that the X direction is defined toward the temporal and nasal directions in the right and left eyes respectively. In order to assess convergence, angle τ of the gaze vector was defined towards the temporal direction of each eye. Hence, $\tau = \alpha$ for the right eye and $\tau = 180° - \alpha$ for the left eye. Figure 2 shows an example of a processed sequence. The variations in gaze angles (τ and β, respectively, in light- and dark-blue asterisks and crosses) and pupillary radius, r (red crosses), are plotted over time, together with the points when the vision condition changed, that is, when the target was presented on the far (magenta vertical lines) and near visual display (black vertical lines).

To evaluate the dynamics of the changes from distance to near vision (FN) and from near to far vision (NF),

the processed curves were subdivided from 1 s before to 3 s after the stimulus change. Then, they were fitted to a hyperbolic tangent function (Equation 5), which provided four parameters (t_m, k, y_i and y_f) that can be related to the physical characteristics of changes. Note that the fitting to Equation (5) does not depend on a by-hand threshold definition, unlike other previous studies.[28–38] The initial (y_i) and final (y_f) steady-state values (i.e., before and after the change) were determined, together with t_m which corresponds to the time when the curve reached the mean value between y_i and y_f, while k refers to the slope of the change:

$$g(t) = \frac{y_i + y_f}{2}\left(1 + \tan h\left[k \bullet \left(t - t_m\right)\right]\right); \quad (5)$$

The fitted curves were derived a second time to define the start and end times (t_i and t_f) from their maximum and minimum peaks, which corresponded to the maximum acceleration and deceleration of the studied parameters, respectively. Therefore, shifts in gaze angle and pupil radius following the stimulus change were characterised by a six-parameter vector. Figure 3 presents the fittings and characterising parameters obtained from one right eye during the NF change. The time was set to zero at the instant when the target was presented on the far vision conditions display.

In Figure 3c, the fitting of the pupil radii obtained following the change from the far to the near conditions and its corresponding characteristic parameters are presented. The grey-shaded area indicates the interval where both fittings were superimposed. The grid time marks during that interval did not match because t = 0 s was set for each subsequent occurence, as the instant when the target was presented on the screen. Due to delays in both the computation and representation of the targets, they were not screened exactly every 4 s (see Figure 2). An additional inequality was the y_f value of the NF fitting not matching the t_i value of the FN phase. This discrepancy was because the different time ranges used before and after the change in the stimulus (1 s before and 3 s after) resulted in different fitting parameters. However, these differences were subsequently averaged.

RESULTS

Data from each eye were captured and processed separately. After ruling out any incorrect measurements and/or incomplete sequences, 108 sequences with gaze vector components and pupil radius data following a change in target position, that is, 3 changes × 9 subjects × 2 eye types (right and left) × 2 change types (NF and FN), were analysed. Each change was defined by the three characteristic vectors from Equation (5) and the subsequent peak detection in the second time derivatives for gaze angle and pupil radius. Table 1 shows the means (standard deviations) for all the parameters.

A two-way analysis of variance (ANOVA) with balanced design was performed to evaluate if eye side (right vs. left) and direction of change (NF and FN) affected the measured time parameters. Analysis of gaze angles τ and β gave p-values of >0.05 (see Table 2) for parameters t_i, t_m and t_f, which indicates that neither of the factors (eye side and direction of change) affected any time parameters for τ and β. Nor was there any evidence for an interaction effect between these factors. The ANOVAs of these time parameters for pupillary radii did not show any significant differences ($p > 0.05$) for the eye side effect and the interaction term but significant differences for the direction of change effect clearly appeared (see Table 2).

As significant differences between the right and left eyes were ruled out, the two subsets were merged and a one-way ANOVA was carried out to evaluate the processes in more depth. This analysis compared the time parameters for τ and β. Parameter t_i did not vary significantly ($p = 0.67$), but p-values of 0.02 and 0.002, respectively, were obtained for t_m and t_f. Figure 4 shows a boxplot of the temporal parameters for gaze vector components τ and β. Note that t_m and t_f were larger for τ than for β. Furthermore, comparison of the time parameters for τ and β to those of the pupil radius was made to show that they were significantly different.

With regard to the slope parameter k, ANOVAs were performed to compare the three variables (τ, β and r) to one another. They all showed significant differences ($p < 0.05$), as shown in Table 3.

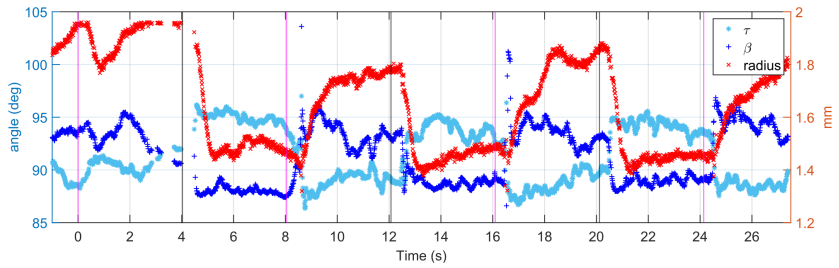

FIGURE 2 Change in gaze angle and pupil radius during an example sequence from a left eye. Time is set at zero at the beginning of the sequence when the target was first presented on the far display. Magenta and black vertical lines mark the points when the target appeared on the far and near displays, respectively. Blue markers represent gaze angles τ and β, and red markers indicate the pupil radius. The left Y-axis corresponds to gaze angles while the right-side Y-axis indicates the pupil radius.

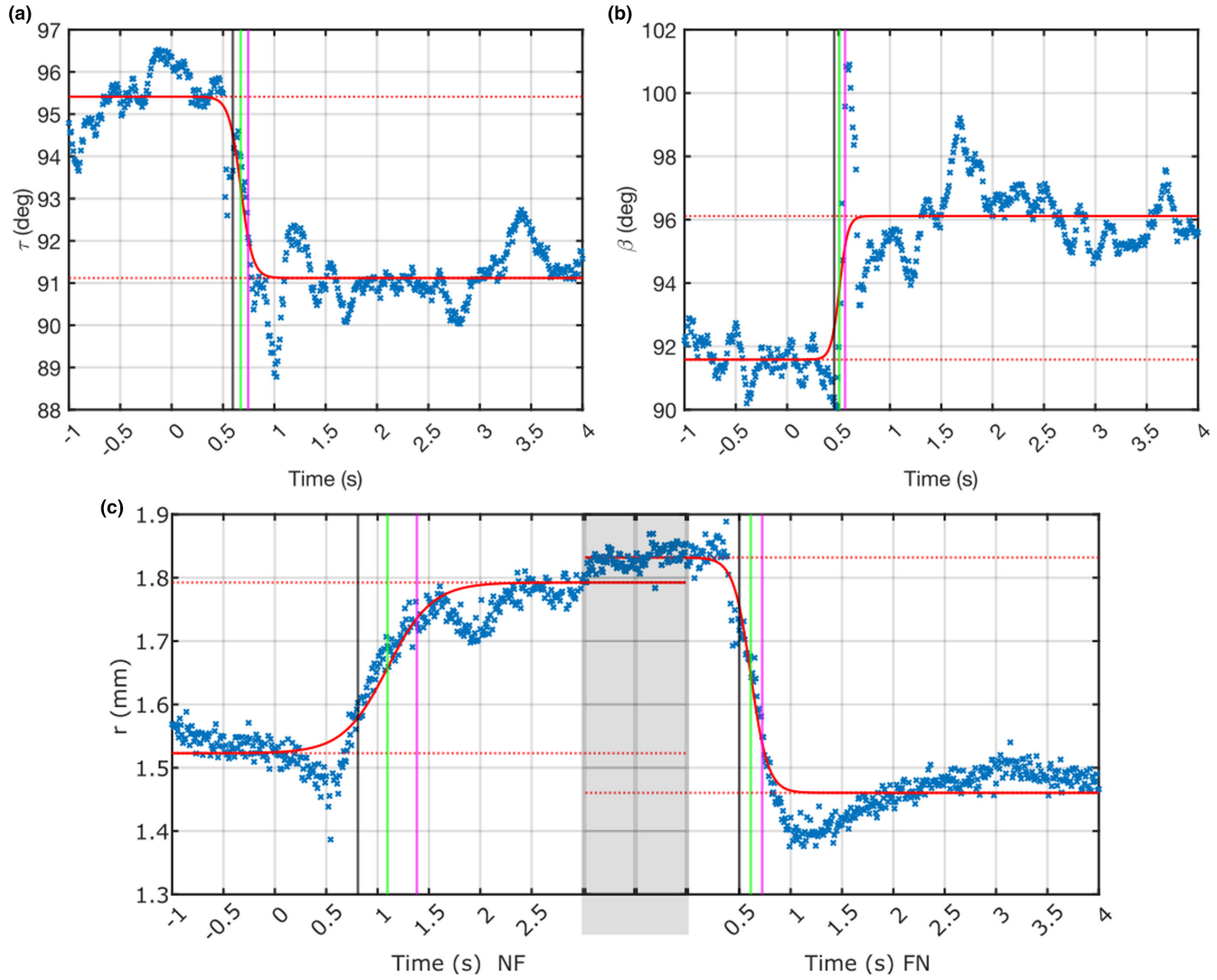

FIGURE 3 Fitting curves (red lines) following Equation (5) for gaze vector components $\tau = 180° - \alpha$ (a) and β (b), obtained from Equation (4), and the pupil radius (c) for a right eye when changing from the near to the far (NF) target ($t = 0$ s). Figure 3c also shows the fitting curve immediately following the change from the far to the near (FN) vision conditions. The grey-shaded area marks the interval where the two fittings are superimposed. The horizontal red dashed lines mark the initial and final steady-state values (y_i and y_f, respectively). The black, green and pink vertical lines correspond to the initial, mean and final times (t_i, t_m and t_f) respectively.

Finally, the steady-state values for the far and near conditions were compared, that is, y_i and y_f. Note that as the final state for NF corresponded to the initial state for FN and vice versa, the parameters from each condition were merged to make comparisons. Figure 5 shows comparison of the far pupillary radii versus the near condition values, together with fitting to the general model $f(x) = ax$. The result of the least square fitting was a parameter with 95% confidence intervals of $a = 1.14$ (1.12, 1.15) with $R^2 = 0.93$ and root mean squared error (RMSE) of 0.14 mm.

The angular components of the gaze vector were analysed in a similar manner to the pupillary radius, albeit with a selected general model, $f(x) = x + b$. The results (95% CI) of fitting were $b_\beta = 4.81°$ (4.47, 5.15) and $b_\tau = -4.98°$ (-5.29, -4.68), with R^2 values of 0.48 and 0.35 and RMSE of 1.77° and 1.59°, respectively. Figure 6 shows both comparisons and their respective least-square fittings.

DISCUSSION AND CONCLUSIONS

A high-speed video-based eye-tracking platform, used to analyse the pupil radius and variations in gaze following a shift in focus between far and near targets, made it possible to determine a number of parameters by fitting to hyperbolic tangent functions. These described not only the dynamics of the muscles involved in the process but also steady-state values under different stimulus conditions.

The overshooting that appeared in the response signals should be noted, specifically in the angular components (Figure 3). This is likely due to the involvement of saccadic movements, which contribute to overshoots in

TABLE 1 Mean (standard deviations) for the start and end times (t_i and t_f, respectively), the time (t_m) when the curve reached the mean value between y_i and y_f (the initial and final steady-states value, respectively) and the slope of the change (k) for the variables (Var.) pupil radius (r) and the gaze vector angles (β and τ convergence angles) following the changes (Chg.) from near to far (NF) and far to near (FN) for each eye (OD, right eye; OS, left eye).

Chg.	Var.	Eye	$t_i(s)$	$t_f(s)$	$t_m(s)$	$k\left(\text{deg}^{-1}\right)$	y_i(deg)	y_f(deg)
NF	τ	OD	0.37 (0.13)	0.60 (0.22)	0.49 (0.13)	30 (50)	95.7 (2.3)	90.9 (2.1)
		OS	0.42 (0.12)	0.58 (0.10)	0.50 (0.10)	13 (12)	95.2 (1.7)	89.7 (1.7)
	β	OD	0.41 (0.14)	0.52 (0.16)	0.46 (0.13)	30 (30)	90.2 (2.1)	95.5 (3.1)
		OS	0.36 (0.07)	0.44 (0.09)	0.40 (0.07)	40 (40)	89.6 (1.3)	94.7 (2.3)
FN	τ	OD	0.41 (0.08)	0.51 (0.11)	0.46 (0.09)	40 (40)	90.5 (2.0)	94.7 (1.8)
		OS	0.38 (0.12)	0.55 (0.11)	0.47 (0.11)	13 (9)	90.0 (2.0)	95.4 (1.7)
	β	OD	0.36 (0.07)	0.44 (0.08)	0.40 (0.07)	60 (50)	94.0 (1.9)	89.7 (1.2)
		OS	0.37 (0.10)	0.48 (0.08)	0.42 (0.07)	40 (30)	94.5 (2.3)	89.9 (1.1)
Chg.	**Var.**	**Eye**	$t_i(s)$	$t_f(s)$	$t_m(s)$	$k\left(\text{mm}^{-1}\right)$	y_i(mm)	y_f(mm)
NF	r	OD	1.3 (0.6)	2.0 (0.6)	1.7 (0.6)	4 (6)	1.9 (0.6)	2.1 (0.5)
		OS	1.1 (0.6)	2.2 (0.6)	1.6 (0.5)	1.6 (0.8)	1.7 (0.5)	2.0 (0.6)
FN	r	OD	0.54 (0.16)	0.78 (0.12)	0.66 (0.12)	7 (4)	2.4 (0.5)	2.0 (0.5)
		OS	0.62 (0.14)	0.83 (0.12)	0.72 (0.13)	6.8 (2.1)	2.1 (0.6)	1.8 (0.5)

TABLE 2 p-Values resulting from the two-way ANOVAs to evaluate the effects of eye side (Eye) and direction of change (Chg.) and their interaction (Int.) over the start time (t_i), the time when the curve reached the mean value between the initial and final steady states (t_m) and the end time (t_f) for the gaze angles (τ and β) and the pupillary radius (r).

	t_i			t_m			t_f		
	τ	β	r	τ	β	r	τ	β	r
Eye	0.34	0.92	0.22	0.30	0.47	0.47	0.39	0.39	0.92
Chg.	0.25	0.99	4×10^{-10}	0.96	0.63	6×10^{-21}	0.31	0.63	7×10^{-25}
Int.	0.18	0.18	0.06	0.70	0.09	0.21	0.68	0.14	0.77

the angular components but may not have a significant impact on pupil dynamics. Hampson et al.[40] employed a fitting procedure using a Boltzmann sigmoidal function to determine the latency of the accommodation response. They disregarded the magnitude of overshooting and fitted the data to a similar function to the hyperbolic tangent function used here. After determining the latency period, they then fitted the responses to a damped sinusoid and extended the analysis to the overshoots. In the present work, the overshoots were also underestimated by the fitting of hyperbolic tangent functions. While it is possible that the absolute amplitude of the response may be slightly underestimated with this approach, it provides a reasonable approximation of the first-order dynamics of the eye movement.

The β angular components of the gaze vector in steady phases can be used to evaluate the angular accuracy of the proposed system. From the comparison plotted in Figure 6a, we obtained $b_\beta = 4.81°$ (95% CI: 4.47, 5.15) and R^2 value of 0.48 and RMSE = 1.77°. This is directly related to the vertical angular difference between the target in the far and near positions, which can be determined as the angular difference between the subtending angles ε_N and ε_F. The average (SD) nasopupillary distance for all the participants was 28.65 mm (1.32). Thus, from Equations (1) and (2), we obtain:

$$\varepsilon_N = 7.0°\,(0.2); \varepsilon_F = 0.93°\,(0.01); \Delta\beta = \varepsilon_N - \varepsilon_F = 6.1°\,(0.2) \quad (6)$$

Note that the theoretical $\Delta\beta$ falls within the confidence limits of b_β defined by the RMSE from the fitting procedure.

The angular component of the gaze vector in the steady-state τ can be used to assess the accommodative response from its relation with convergence. From the fitting shown in Figure 6b, the obtained convergence was $C(\text{SD}) = -2b_\tau \cong 10°\,(3)$. Assuming all of the change was due to accommodative convergence and proximal vergence did not vary, then convergence would correspond to an accommodative convergence of $AC(\text{SD}) = 18\,\Delta\,(5)$. Under that assumption, the accommodative response can be theoretically set as $A = 2.4$ D, and therefore, AC/A can be obtained as follows:

$$\frac{\text{AC}}{A} = \frac{18\ (5)}{2.4} = 7.5\ (2.1)(\Delta\ /\ \text{D}); 5 - 10{:}\,1; \quad (7)$$

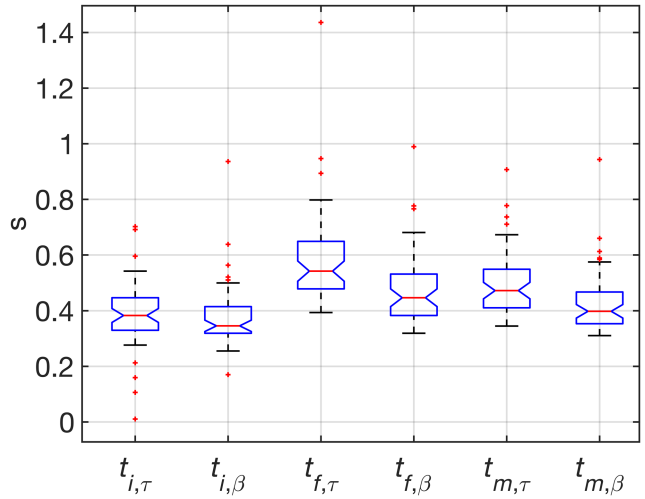

FIGURE 4 Boxplot of temporal parameters start time (t_i), the time when the curve reached the mean value between the initial and final steady states (t_m) and the end time (t_f) for the gaze vector components (τ and β, added to the different time parameters as subindexes). The *Y*-axis indicates the time in seconds.

TABLE 3 *p*-Values resulting from the ANOVAs comparing the slope parameter *k* obtained for the gaze vector components (τ and β) and the pupillary radius (*r*) for both directions of change (NF, near to far; and FN, far to near).

	β	*r*
τ		
NF	3×10^{-3}	1×10^{-5}
FN	6×10^{-3}	9×10^{-6}
β		
NF		2×10^{-11}
FN		4×10^{-11}

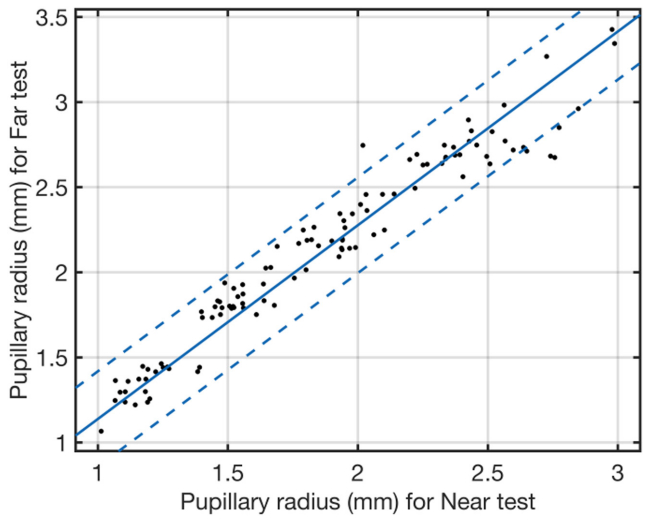

FIGURE 5 Steady-state pupillary radius for the far vision conditions versus the corresponding value for the near condition (black dots) together with fitting (blue line) to the general model $f(x) = ax$ and the 95% prediction boundaries (dashed blue lines).

As the proposed setup can provide closed-loop response measurements, with convergence due to both accommodative convergence and proximal vergence, then the close-loop response can be related to an AC/*A* ratio of 6:1 with a normal range of 4–8:1.[9] By making comparison to the AC/*A* ratio calculated in Equation (7), it is concluded that the proposed method provides an approximate accommodative measurement of the accommodative response.

The measured pupillary responses indicate that the pupil radius for the far condition was 1.14 (0.14) times larger than that for the near condition, as depicted in Figure 5. These findings are consistent with Kubota et al.,[48] who reported that the maximum pupillary diameter was 1.25 (0.42)-fold bigger than the minimum diameter when considering an accommodative response of 4.04 (2.00) D for a group of individuals <45 years of age. Similarly, Subbaram and Bullimore[45] reported a factor of 1.12 (0.36) times between the maximum and minimum pupillary diameters of 30 emmetropes using a 2D stimulus.

Analysis of factors (eye side and direction of change, i.e., NF or FN) that might affect time parameters describing the changes between the far and near targets did not reveal significant differences for any of the variables (α, β, and *r*) or a significant interaction. While the time parameters for gaze angle also showed no significant differences between the direction of change, significant differences for the change type effect on the pupil radius were clearly indicated, as shown by the *p*-values presented in Table 2.

Differences in the dynamics of pupillary constriction and dilation were probably due to the distinct nerve and muscle forces involved in each process. Pupillary constriction (miosis) during accommodation involves the iris sphincter muscle, which is parasympathetically innervated via the short ciliary nerves. The parasympathetic fibres that serve the sphincter muscle originate from the Edinger–Westphal nucleus of cranial nerve III. The signal synapses in the ciliary ganglia terminate on the muscarinic receptors within the muscle. Sympathetic innervation from the superior cervical ganglia is responsible for dilation by helping to relax the sphincter muscle. This innervation projects to the iris dilator muscle via the long ciliary nerves to control pupil dilation.[49] The sphincter muscle contracts the pupil in a circular motion, while the dilator muscles enlarge the pupil by expanding the iris radially.[50] By comparing the temporal parameters obtained for the pupillary responses, as presented in Table 1, it may be observed that the NF change was larger than the FN change ($p < 0.001$). Moreover, the slope parameter *k* was smaller for NF shifts than for FN. This implies that miosis is faster than mydriasis during the accommodation/disaccommodation process, much like the pupillary response to light.

Temporal parameters for the three variables were compared. The pupil radius measurements were longer than the gaze vector components (see Table 1). The latter were compared with one another, and while no significant difference was found for the latency t_i of τ and β, significant differences were observed for t_f and t_m. These differences can

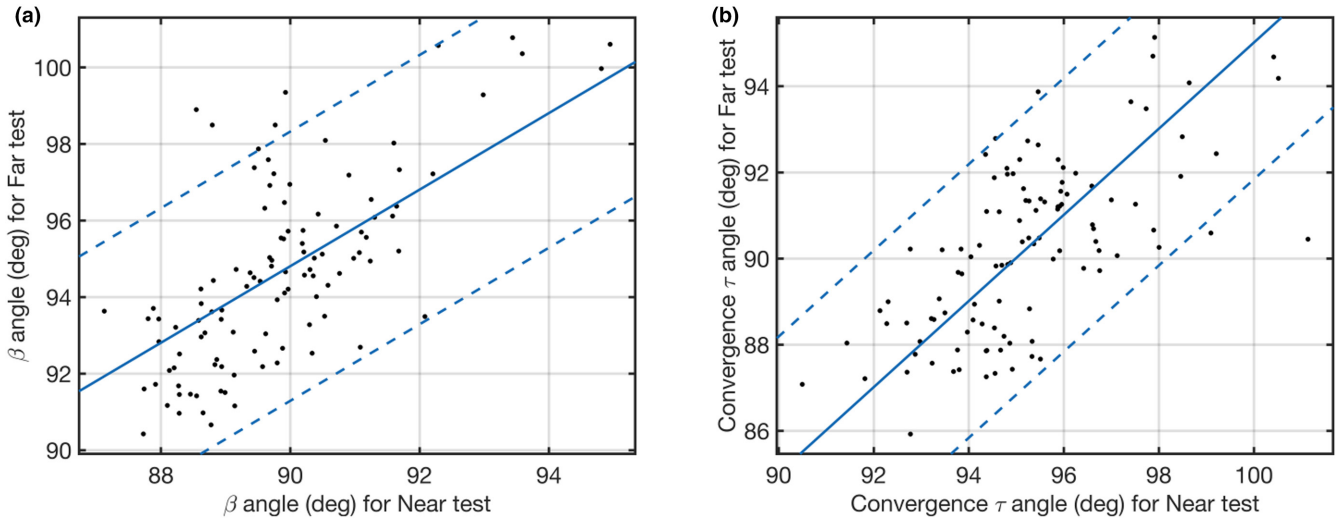

FIGURE 6 (a) The steady-state β angle and (b) the convergence τ angle for the far versus the near condition (black dots) together with fitting (blue line) to the general model $f(x) = x + b$ and the 95% prediction boundaries (dashed blue lines).

be attributed to the fact that τ is related to convergence, whereas β relates to saccades due to the vertical change in the position of the near and far targets. Indeed, it can be concluded from Figure 4 and Table 1 that t_f and t_m are shorter for β than for τ, which is consistent with the finding that accommodative responses take longer than eye movements,[31] even though their latencies are the same. Comparison of the k values lead to the same conclusion because the values for the τ angle were lower than those for β, which implies that the vertical component of the gaze vector changes more quickly than the horizontal component.

A comprehensive analysis of the three-component near reflex by simultaneously measuring pupillary changes, convergence and accommodation when switching between distance and near fixation is presented. A calibration process was developed and a set of parameters were computed to describe the dynamics of both processes. This comprehensive approach included an analysis of the interrelation among these three components, provided a more complete understanding of the near reflex and contributes to the existing literature by examining the intricate dynamics of the accommodative process.

One of the noteworthy features of this system is the simultaneous measurement of eye convergence or divergence and pupil size under natural viewing conditions. This aspect sets the present study apart from previous research that has often employed subjective or objective techniques in controlled laboratory settings. By capturing these parameters in real-world scenarios, this study not only advanced our understanding of the adaptive mechanisms of the visual system and vergence dynamics but also has practical implications for clinical diagnosis and research.

AUTHOR CONTRIBUTIONS

Julián Espinosa: Conceptualization (equal); investigation (equal); methodology (lead); project administration (lead); resources (equal); supervision (equal); writing – original draft (equal). **Kauzar Archid:** Data curation (equal); formal analysis (equal); investigation (equal); software (equal); visualization (equal). **Jorge Pérez:** Conceptualization (equal); formal analysis (equal); methodology (equal); validation (equal); writing – review and editing (equal). **Esther Perales:** Conceptualization (equal); investigation (equal); project administration (equal); software (equal); writing – review and editing (equal).

FUNDING INFORMATION

This work was funded by Universidad de Alicante, participating CRUE-CSIC institution.

CONFLICT OF INTEREST STATEMENT

The authors certify that they have no affiliations with or involvement with any organisation or entity with any financial interest in this work, and have no financial interest in the subject matter or materials discussed in this manuscript.

ORCID

Julián Espinosa https://orcid.org/0000-0001-6817-3117

REFERENCES

1. Folk ER. Vergence eye movements: basic and clinical aspects. *Arch Ophthalmol*. 1984;102:342–4.
2. Bharadwaj SR, Roy S, Satgunam P. Spasm of near reflex: objective assessment of the near-triad. *Invest Ophthalmol Vis Sci*. 2020;61:ARVO E-Abstract 18.
3. Dragoi V. Chapter 7: Ocular Motor System. Neuroscience online: An electronic textbook for the neurosciences. Department of Neurobiology and Anatomy, The University of Texas Medical School at Houston. [cited 2023 Feb 10]. Available from: https://nba.uth.tmc.edu/neuroscience/s3/chapter07.html
4. Motlagh M, Geetha R. Physiology, accommodation. StatPearls [Internet]. Treasure Island, FL: StatPearls Publishing; 2022. [cited 2023 Feb 10]. Available from: http://www.ncbi.nlm.nih.gov/books/NBK542189/
5. Fincham EF, Walton J. The reciprocal actions of accommodation and convergence. *J Physiol*. 1957;137:488–508.

6. Schor C. Fixation of disparity: a steady state error of disparity-induced vergence. *Am J Optom Physiol Opt*. 1980;57:618–31.
7. Semmlow J, Heerema D. The synkinetic interaction of convergence accommodation and accommodative convergence. *Vision Res*. 1979;19:1237–42.
8. Tsuetaki TK, Schor CM. Clinical method for measuring adaptation of tonic accommodation and vergence accommodation. *Optom Vis Sci*. 1987;64:437–49.
9. Hughes A. AC/A ratio. *Br J Ophthalmol*. 1967;51:786–7.
10. Jones R. Fusional vergence: sustained and transient components. *Am J Optom Physiol Opt*. 1980;57:640–4.
11. Hung GK, Semmlow JL, Ciuffreda KJ. A dual-mode dynamic model of the vergence eye movement system. *IEEE Trans Biomed Eng*. 1986;33:1021–8.
12. Semmlow JL, Hung GK, Ciuffreda KJ. Quantitative assessment of disparity vergence components. *Invest Ophthalmol Vis Sci*. 1986;27:558–64.
13. Semmlow JL, Yaramothu C, Scheiman M, Alvarez T. Vergence fusion sustaining oscillations. *J Eye Mov Res*. 2021;14. https://doi.org/10.16910/jemr.14.1.4
14. Yuan W, Semmlow JL, Alvarez TL, Munoz P. Dynamics of the disparity vergence step response: a model-based analysis. *IEEE Trans Biomed Eng*. 1999;46:1191–8.
15. Erkelens CJ, Van der Steen J, Steinman RM, Collewijn H. Ocular vergence under natural conditions. I. Continuous changes of target distance along the median plane. *Proc R Soc Lond B Biol Sci*. 1989;236:417–40.
16. Crawford JD, Vilis T. Symmetry of oculomotor burst neuron coordinates about Listing's plane. *J Neurophysiol*. 1992;68:432–48.
17. Mutti DO, Mitchell GL, Moeschberger ML, Jones LA, Zadnik K. Parental myopia, near work, school achievement, and children's refractive error. *Invest Ophthalmol Vis Sci*. 2002;43:3633–40.
18. Gwiazda JE, Hyman L, Norton TT, Hussein MEM, Marsh-Tootle W, Manny R, et al. Accommodation and related risk factors associated with myopia progression and their interaction with treatment in COMET children. *Invest Ophthalmol Vis Sci*. 2004;45:2143–51.
19. Saw SM, Nieto FJ, Katz J, Chew SJ. Distance, lighting, and parental beliefs: understanding near work in epidemiologic studies of myopia. *Optom Vis Sci*. 1999;76:355–62.
20. Newman NJ, Biousse V, Kerrison JB, Miller NR, Walsh FB, Hoyt WF. Walsh and Hoyt's clinical neuro-ophthalmology. Philadelphia, PA: Lippincott Williams & Wilkins; 2004. p. 1163.
21. Rabbetts RB. Bennett and Rabbett's clinical visual optics. 4th ed. Edinburgh: Elsevier/Butterworth Heinemann; 2007.
22. Benjamin WJ. Borish's clinical refraction. 2nd ed. Oxford: Butterworth-Heinemann; 2006.
23. Aldaba M, Gómez-López S, Vilaseca M, Pujol J, Arjona M. Comparing autorefractors for measurement of accommodation. *Optom Vis Sci*. 2015;92:1003–11.
24. Win-Hall DM, Glasser A. Objective accommodation measurements in prepresbyopic eyes using an autorefractor and an aberrometer. *J Cataract Refract Surg*. 2008;34:774–84.
25. Tarrant J, Roorda A, Wildsoet CF. Determining the accommodative response from wavefront aberrations. *J Vis*. 2010;10:4. https://doi.org/10.1167/10.5.4
26. López-Gil N, Iglesias I, Artal P. Retinal image quality in the human eye as a function of the accommodation. *Vision Res*. 1998;38:2897–2907.
27. Aldaba M, Vilaseca M, Díaz-Doutón F, Arjona M, Pujol J. Measuring the accommodative response with a double-pass system: comparison with the Hartmann–Shack technique. *Vision Res*. 2012;62:26–34.
28. Kasthurirangan S, Vilupuru AS, Glasser A. Amplitude dependent accommodative dynamics in humans. *Vision Res*. 2003;43:2945–56.
29. Bharadwaj SR, Schor CM. Dynamic control of ocular disaccommodation: first and second-order dynamics. *Vision Res*. 2006;46:1019–37.
30. Suryakumar R, Meyers JP, Irving EL, Bobier WR. Application of video-based technology for the simultaneous measurement of accommodation and vergence. *Vision Res*. 2007;47:260–8.
31. Campbell FW, Westheimer G. Dynamics of accommodation responses of the human eye. *J Physiol*. 1960;151:285–95.
32. Tucker J, Charman WN. Reaction and response times for accommodation. *Am J Optom Physiol Opt*. 1979;56:490–503.
33. Charman WN. Chapter 1 The retinal image in the human eye. *Prog Retin Res*. 1983;2:1–50.
34. Heron G, Winn B. Binocular accommodation reaction and response times for normal observers. *Ophthalmic Physiol Opt*. 1989;9:176–83.
35. Culhane HM, Winn B. Dynamic accommodation and myopia. *Invest Ophthalmol Vis Sci*. 1999;40:1968–74.
36. Heron G, Charman WN, Schor C. Dynamics of the accommodation response to abrupt changes in target vergence as a function of age. *Vision Res*. 2001;41:507–19.
37. Chirre E, Prieto P, Artal P. Dynamics of the near response under natural viewing conditions with an open-view sensor. *Biomed Opt Express*. 2015;6:4200–11.
38. Ghoushchi VP, Mompeán J, Prieto PM, Artal P. Binocular dynamics of accommodation, convergence, and pupil size in myopes. *Biomed Opt Express*. 2021;12:3282–95.
39. Fernández EJ, Artal P. Study on the effects of monochromatic aberrations in the accommodation response by using adaptive optics. *J Opt Soc Am A*. 2005;22:1732–8.
40. Hampson KM, Chin SS, Mallen EAH. Effect of temporal location of correction of monochromatic aberrations on the dynamic accommodation response. *Biomed Opt Express*. 2010;1:879–94.
41. Kasthurirangan S, Glasser A. Age related changes in the characteristics of the near pupil response. *Vision Res*. 2006;46:1393–1403.
42. Jainta S, Jaschinski W. Individual differences in binocular coordination are uncovered by directly comparing monocular and binocular reading conditions. *Invest Ophthalmol Vis Sci*. 2012;53:5762–9.
43. Charman WN, Radhakrishnan H. Accommodation, pupil diameter and myopia. *Ophthalmic Physiol Opt*. 2009;29:72–9.
44. Pupil Core. Open source eye tracking platform—Pupil Labs [Internet]. [cited 2023 Feb 17]. Available from: https://pupil-labs.com/products/core/
45. Subbaram MV, Bullimore MA. Visual acuity and the accuracy of the accommodative response. *Ophthalmic Physiol Opt*. 2002;22:312–8.
46. Lu F, Qu J, Yan J, Xu D, Jiang BC. Accommodative response—a comparison of emmetropia and anisometropia. *Invest Ophthalmol Vis Sci*. 2004;45:ARVO E-Abstract 1737.
47. Absolute Orientation—Horn's method [Internet]. [cited 2023 Jan 10]. Available from: https://ch.mathworks.com/matlabcentral/fileexchange/26186-absolute-orientation-horn-s-method
48. Kubota M, Kubota S, Kobashi H, Ayaki M, Negishi K, Tsubota K. Difference in pupillary diameter as an important factor for evaluating amplitude of accommodation: a prospective observational study. *J Clin Med*. 2020;9:2678. https://doi.org/10.3390/jcm9082678
49. McDougal DH, Gamlin PD. Autonomic control of the eye. *Compr Physiol*. 2015;5:439–73.
50. Bloom J, Motlagh M, Czyz CN. Anatomy, head and neck, eye iris sphincter muscle. StatPearls [internet]. Treasure Island, FL: StatPearls Publishing; 2022. [cited 2023 Feb 8]. Available from: http://www.ncbi.nlm.nih.gov/books/NBK532252/

How to cite this article: Espinosa J, Archid K, Pérez J, Perales E. Using a video-based eye tracker to analyse the binocular near-reflex dynamics response. *Ophthalmic Physiol Opt*. 2023;43:1540–1549. https://doi.org/10.1111/opo.13203